energies

MDPI

Article

Quenching Experiments with CrAl-coated Zircaloy Cladding in Reflooding Water Flows

Wang Kee In * and Kwan Geun Lee

Innovative SMR Development, Korea Atomic Energy Research Institute, 989-111 Daedeok-daero, Yuseong-Gu, Daejeon 34057, Korea; jr6203@naver.com

* Correspondence: wkin@kaeri.re.kr; Tel.: +82-42-868-2823

Abstract: A quenching experiment is performed to investigate the heat transfer characteristics and cooling performance of CrAl-coated Zircaloy (Zr) cladding in a water flow. The CrAl-coated Zr cladding is one of the accident tolerant fuels for light water reactors. The uncoated Zr cladding is also used in this quenching experiment for comparison. This experiment simulates reflood quenching of fuel rod during loss of coolant accident (LOCA) in nuclear power plant. The test conditions were determined to represent the peak cladding temperature, the coolant subcooling and the reflood velocity in the event of LOCA. The flow visualization showed the film boiling during early stage of reflood quenching and the transition to nucleate boiling. The film layer decreases as the coolant subcooling increases and becomes wavy as the reflood velocity increases. The CrAl-coated Zr cladding showed more wavy and thinner film than the uncoated Zr cladding. The rewetting temperature increases as the initial wall temperature and/or the coolant subcooling increases. The quench front velocity increases significantly as the coolant subcooling increases. The reflood velocity has a negligible effect on rewetting temperature and quench front velocity.

Keywords: quenching; reflood; CrAl-coated Zr; cladding; quench curve; rewetting temperature; speed of quench front

Citation: In, W.K.; Lee, K.G. Quenching Experiments with CrAl-coated Zircaloy Cladding in Reflooding Water Flows. *Energies* **2021**, *14*, 1859. https://doi.org/10.3390/en14071859

Academic Editor: Enrico Nobile

Received: 9 March 2021
Accepted: 24 March 2021
Published: 26 March 2021

1. Introduction

The zirconium-based cladding of fuel rods in nuclear reactors generates a large amount of hydrogen and heat due to the chemical reaction between zirconium and steam, particularly during any loss of the active cooling system. A hydrogen explosion occurred after the complete loss of the emergency core cooling system due to the station blackout at the Fukushima Daiichi nuclear power plant in 2011. Accident-tolerant fuels (ATFs) have been proposed to replace the zirconium-based cladding and uranium dioxide (UO_2) fuel in light water reactors (LWRs). Zinkle et al. [1] discussed the perspectives of ATFs for LWRs, which can enhance the safety margins for nuclear power systems. Kurata [2] identified the research and development metrics and the attributes of candidate ATF-concepts. The ATFs can be categorized into the modification of Zr cladding, the non-Zr cladding (FeCrAl alloy, silicon carbide composite) and the alternative fuel forms (fully ceramic microencapsulated fuel). Hence, the ATF claddings were developed for improving oxidation resistance and mechanical strength.

There are numerous studies of the ATF concepts focusing on fabrication technique and material performances [3–12]. However, there have been a limited number of studies on the thermal-hydraulic performance of the ATF cladding which is essential to evaluate the enhancement of safety margin under accident conditions. The CrAl-coated Zr cladding was proposed as the ATF candidate for near-term employment of ATFs in LWRs because of fabrication and neutron economics. Kim et al. [12] developed an arc-ion plating technique for CrAl coating and laser-beam scanning for oxide dispersion strengthened (ODS) treatment. The out-of-pile testing of the CrAl-coated Zr cladding showed the sufficient

potential as an ATF cladding by improving oxidation resistance and mechanical strength at high temperature.

Seshadri and Shirvan [13] experimentally analyzed the cooling performance of various coating materials on Zircaloy-4 (Zry-4) rods. The coating materials are chromium, FeCrAl, and molybdenum. The rod specimens were quenched in water at saturation temperature. The FeCrAl coated Zry-4 rod showed better cooling performances compared to uncoated Zry-4 rod. Lee et al. [14] conducted critical heat flux (CHF) experiments with tube specimens for FeCrAl alloy, Zry-4 and Inconel 600. The FeCrAl alloy showed a more than 10% increase in CHF compared to Zry-4 and Inconel 600.

Kang et al. [15] performed a quenching experiment with a vertical rod for ATF cladding candidates, i.e., FeCrAl and SiC-chemical vapor deposition (CVD). They analyzed the minimum film boiling temperature (MFBT), minimum heat flux and the heat transfer coefficient of film boiling. Wang et al. [16] investigated the Leidenfrost phenomena of droplet impact on heated SiC-CVD surface. They developed an empirical model for droplet maximum spreading factor. Wang et al. [17] performed the experimental investigation on the transient film boiling heat transfer of FeCrAl rod quenched in water. They reported that the quenching time and MFBT are influenced by surface roughness and surface wettability as well as by the liquid subcooling.

Recently, Lee et al. [18] carried out a quenching experiment with tube specimens for Cr-alloy-coated Zr cladding at 600 °C in a water pool. The Cr-alloy-coated Zr cladding showed quenching performance, e.g., quenching time and MFBT, similar to that of an uncoated Zr cladding. They also found that the quenching time is shorter for thinner coating. However, this experiment does not represent the reflooding of emergency core cooling water and the peak cladding temperature (PCT) in the event of LOCA. Hence, a reflood quenching experiment is still required to assess the cooling performance and interface integrity of the Cr-alloy-coated Zr cladding during LOCA reflooding.

The objective of this study was to evaluate the cooling performance of CrAl-coated Zr cladding in comparison with the Zr cladding during reflood quenching in a water flow. The LOCA analysis for commercial PWR showed the reflooding velocity of 0.02 m/s–0.1 m/s and the PCT higher than 600 °C. This paper presents the effects of initial cladding temperature (600 °C and 800 °C), liquid subcooling (5 °C–50 °C) and reflood velocity (0.02 m/s–0.1 m/s). The transient cladding temperature was measured using K-type thermocouples, and the quenching process was visualized by high-speed camera and digital camera. Scanning electron microscope (SEM) images of cladding specimens were taken before and after quenching tests. The rewetting temperature and speed of quench front were estimated from quench curves and visualized images of reflood quenching.

2. Experimental Methods and Procedure

2.1. Experimental Apparatus and Setup

Figure 1 illustrates the schematic of the experimental apparatus for reflood quenching of cladding specimens. The quenching apparatus consists of test section, electrical heating element, coolant supply equipment, data acquisition system (DAS) and flow visualization system. The test section is a vertical tube specimen (uncoated and CrAl-coated Zr claddings) with quartz shroud. The heating element is made of tungsten rod and ceramic tube. The tungsten rod is heated by a direct current (DC) power supply with copper bars at the lower and upper ends. The ceramic tube is used for mounting thermocouples and isolating electrical current. In order to prevent equipment damage due to high temperature of cladding specimen, two cooling chambers are installed at the bottom and top sections of tube specimen. A constant-temperature bath circulates cooling water through the bottom and top chambers.

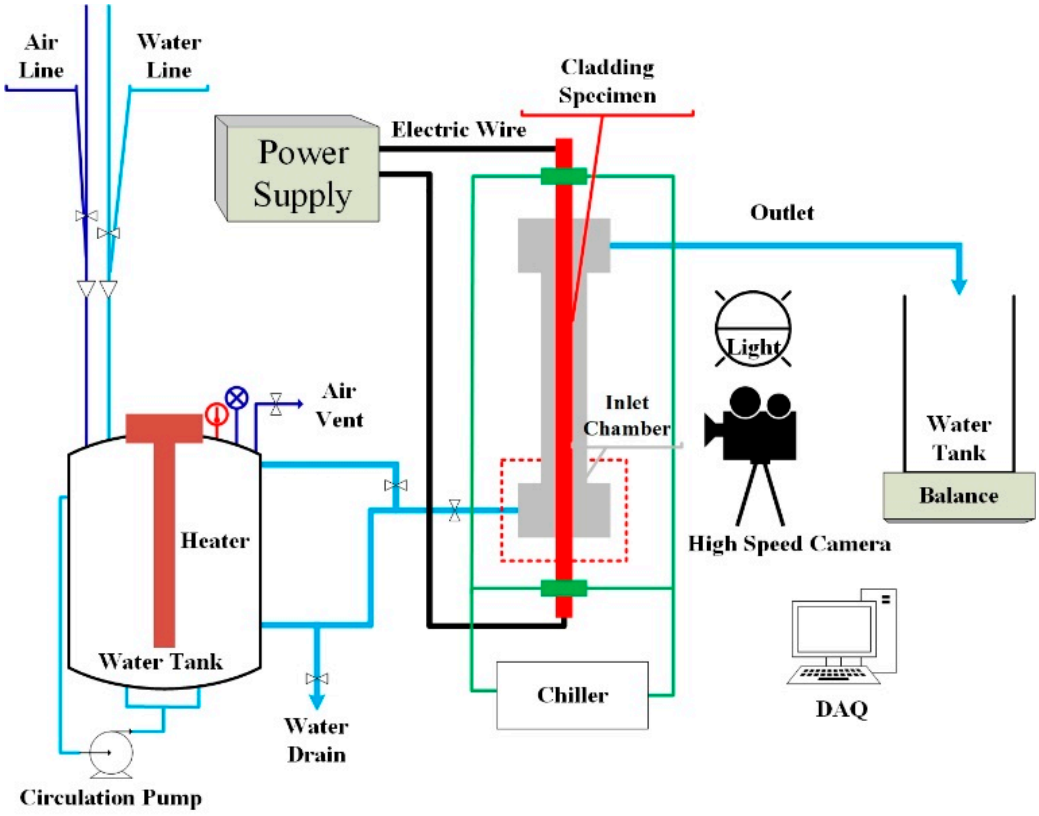

Figure 1. Schematic of experimental apparatus for reflood quenching.

The coolant supply system consists of a water tank, deionized (DI) water generator and pressure regulator. The pressure in the water tank is kept at constant by compressed air which is controlled by a pressure regulator. The water temperature is controlled by a heater inside water tank. The cooling water in the water tank is mixed using a recirculating pump to prevent thermal stratification. Thermal insulation and heating tape are used in the pipelines from the water tank to the test section in order to minimize the drop of coolant temperature due to heat losses. The cooling water is discharged into the drain tank through three outlets. The mass flow rate of coolant is measured using weight of discharged cooling water for constant duration.

The data acquisition system is established using a Labview program to acquire the coolant temperature and the cladding temperature in real time. The K-type thermocouples (0.05 mm in diameter) are installed at the inlet chamber of test section and the cladding tube. A data acquisition device (9213 and 9221, National Instruments, Texas, USA) is used to process the thermocouple readings in every 0.2 s. The thermocouples (TCs) are calibrated using a calibrator (FLUKE, WA, USA) and the temperature measurement error is estimated to be ± 3.7 °C

A high-speed camera (FASTCAM SA3, Photron, CA, USA) is used to visualize the quenching at 500 frames per second (fps) in 512×1024 pixels. Since the recording time of high speed camera is short due to memory limit, a digital camera is also used to record whole process of reflood quenching at 30 fps. A Phoenix 300 device (Kromtek, Malaysia) is used to measure the contact angle on the surface of cladding specimens before and after the experiment. The measurement accuracy of contact angle is 0.1°. The surface roughness was also measured using a SJ-201 device (Mitutoyo, Kanagawa, Japan) with resolution of 0.02 μm. Table 1 lists the sensors and equipment used in this experiment.

Table 1. Summary of sensors and equipment.

Type/Device	Measuring Parameter	Accuracy
K-type TC	Temperature	±3.7 °C
Electronic scale, EK6100i	Flowrate	0.1 g
High-speed camera, FASTCAM SA3	Flow pattern	500 fps @512 × 1024 pixels
Digital camera, SONY alpha 6400	Flow pattern	30 fps @4K pixels
Phoenix 300	Contact angle	0.1°
Mitutoyo SJ-201	Surface roughness	0.02 μm

2.2. Test Specimen

The test specimen shown in Figure 2 consists of a cladding tube, ceramic tube and tungsten rod. The ceramic tube is used to electrically isolate the cladding tube from the tungsten rod. The four TCs are placed in between ceramic tube and cladding tube. It is noted that four TCs (TC1-4) are installed in three axial locations with two TCs in the center of tube specimen. The axial distance between the TCs is 40 mm. The outer diameter, thickness and length of uncoated Zr cladding are 9.5, 0.57 and 400 mm, respectively. The diameter and length of tungsten rod is 4 and 500 mm.

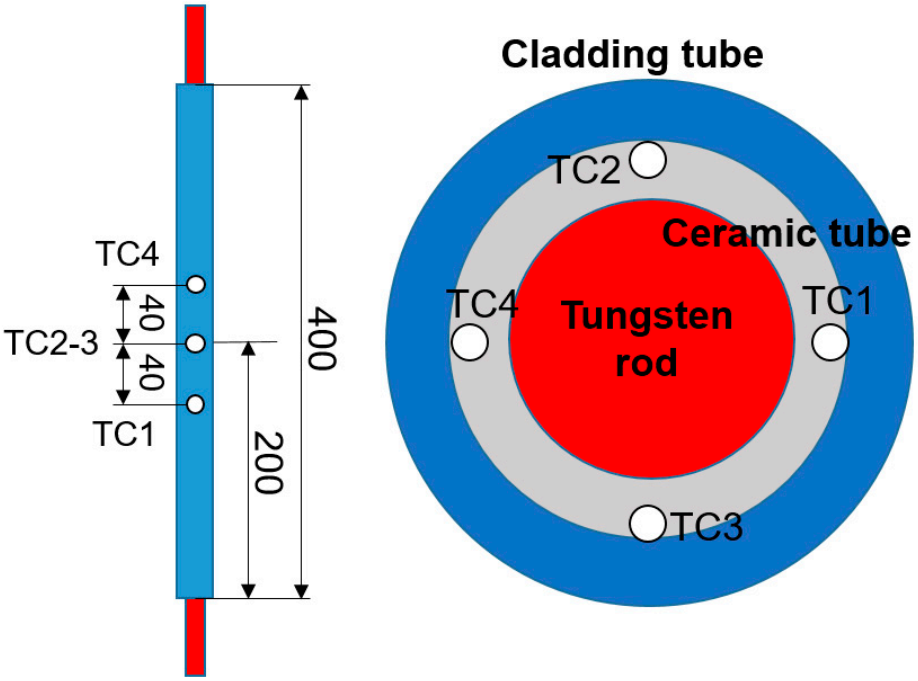

Figure 2. Schematic of test specimen and TC location.

The CrAl-coated Zr cladding was fabricated by an arc-ion plating technique which is known as a high-energy deposition method providing excellent film density and economic efficiency [12]. The thickness of the CrAl coating layer is approximately 50 μm. The coated specimen is polished using #2400 mesh sandpaper. The mean surface roughness (Ra) is 0.19 μm and 1.3 μm for uncoated and CrAl-coated cladding specimens, respectively.

Figure 3 shows the contact angle (θ for Zr and CrAl-coated Zr claddings before the quench experiment. The measured contact angle is 66 deg. and 57 deg. for Zr cladding and CrAl-coated Zr cladding, respectively. The CrAl-coated Zr cladding appears to be slightly more hydrophilic than the Zr cladding.

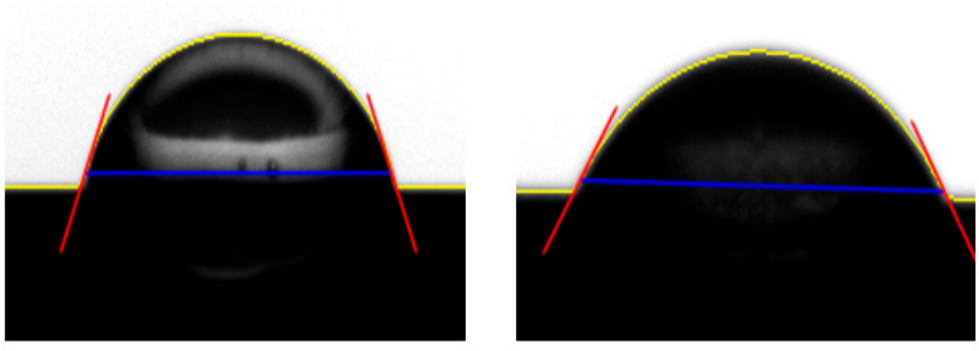

(**a**) (**b**)

Figure 3. Contact angle of as-received specimen for; (**a**) Zr cladding (θ = 66°); (**b**) CrAl-coated Zr cladding (θ = 57°).

Figure 4 compares the cross-sectional SEM images for Zr and CrAl-coated Zr claddings after quenching test. The SEM image in Figure 4a is the Zr specimen after six times quenching tests at 600 °C. Figure 4b shows the SEM image of CrAl-coated Zr specimen after eight and six quenching tests at 600 °C and 800 °C, respectively. The Zr specimen shows an oxide layer of 3.93 μm thickness on the outer surface. It was also found that the oxide layer for Zr specimen increases as the quenching test is repeated. The CrAl-coated specimen in Figure 4b shows the coating layer of 50 μm on the outer surface of Zr cladding but no oxide layer. This indicates that the CrAl-coated Zr cladding is highly resistant to high temperature oxidation as designed.

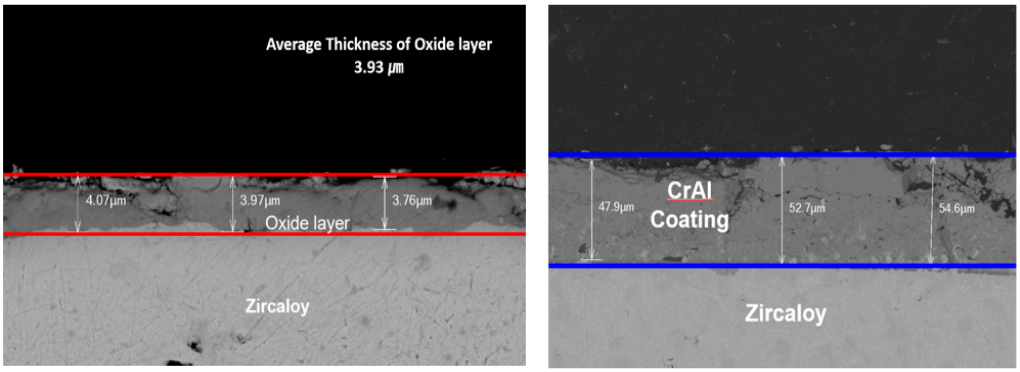

(**a**) (**b**)

Figure 4. SEM photographs after quenching test for; (**a**) Zr cladding; (**b**) CrAl-coated Zr cladding.

2.3. Test Conditions and Procedure

This experiment is performed to evaluate the cooling performance of CrAl-coated Zr cladding during reflood quenching of LOCA in a pressurized water reactor (PWR). The experimental conditions depend on initial cladding temperature, coolant subcooling and reflood flowrate. The initial cladding temperatures (Tw) are 600 °C and 800 °C. The coolant temperature is changed from 50 °C to 95 °C. Since the saturation temperature of coolant (water) is 100 °C at 1 atm, the coolant subcooling (T_{sub}) ranges from 5 °C to 50 °C. The reflood flowrate of coolant is adjusted to vary the reflood velocity (Vc) from 0.02 m/s to 0.1 m/s, which simulates low and high reflood velocity during LOCA in PWR. Table 2 lists the summary of test conditions.

Table 2. Summary of test conditions.

Parameter	Unit	Value
Initial cladding temperature	°C	600, 800
Coolant temperature	°C	50–95
Reflood velocity	m/s	0.02, 0.05, 0.1

The water tank is filled with DI water and the water temperature is maintained at the target temperature using an electrical heater. A water pump recirculates the DI water in water tank from bottom to top in order to prevent thermal stratification. The coolant pipeline from water tank to test section is thermally insulated and heated by ribbon heater in order to maintain the coolant temperature at target value. The electrical current of DC power supply for tungsten rod increased continually such that the cladding temperature reaches its target temperature. Figure 5 illustrates the heat-up of CrAl-coated Zr cladding. It took approximately 700 s for the cladding temperature to reach 800 °C. During the heat up of test specimen, the bottom and top cooling chambers are cooled down by circulating cold water from the water bath at constant temperature, i.e., 7 °C.

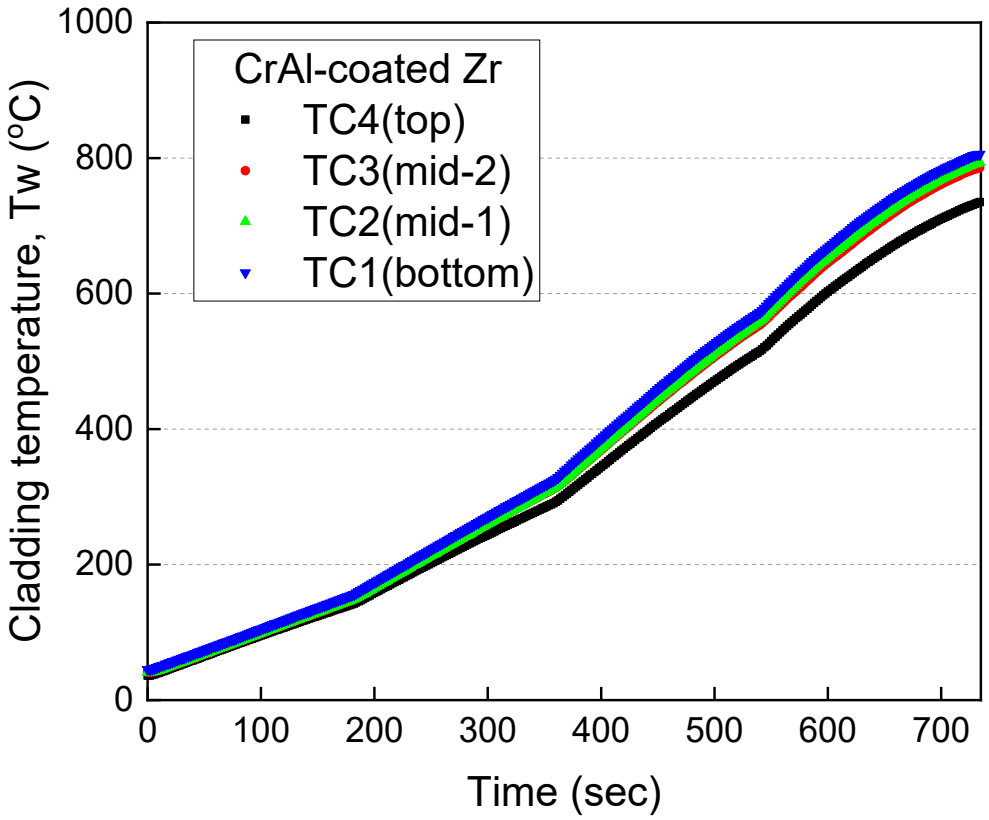

Figure 5. Electrical heat-up of CrAl-coated Zr cladding.

The water tank is pressurized with compressed air at constant pressure. The position of the gate valve in the coolant pipeline is adjusted to control the coolant flow rate at the target reflood velocity. Once the cladding specimen reaches its target temperature, the cooling water in compressed tank is injected into test section by opening the on/off valve in the pipeline. The data acquisition system acquires the coolant temperature at the inlet of test section as well as the cladding temperature in real time (0.2 s) during quenching test.

A high-speed camera and a digital camera are used to visualize two-phase flow pattern during quenching test. The high-speed camera captures the fine structure of the two-phase flow pattern near the quench front. The digital camera visualizes the quenching process in

the whole region of the active test section. The DC power for heater rod is turned off when the cladding temperature is lower than approximately 200 °C. The quenching experiment is complete when the cladding specimen is cooled down to the coolant temperature.

3. Experimental Results and Discussions

3.1. Flow Visualization of Reflood Quenching

The digital camera records dynamic images of flow transition from bottom to top of test section during quenching experiments. The high-speed camera captures the flow images in the local region of test section. The videos taken using the digital and high-speed cameras are converted into still pictures. In the early stage of quenching, a vapor film develops on the outer surface of tube specimen due to the high cladding temperature. The vapor film is collapsed by a quench front that goes up from the bottom of the test section. The bubbly flow is observed to follow the film flow. Then, the reflood quenching ends up with single-phase convective flow as the quench front reaches the top of test section.

Figure 6 shows the digital and high-speed camera pictures for the Zr specimen quenching at Tw = 800 °C, T_{sub} = 5 °C and Vc = 0.05 m/s. The digital-camera image at 0 s shows a cloud of bubbles in lower region below the water level indicated by a white line. The digital-camera picture at 25 s shows the quench front (dotted line) in the bottom region and the collapse of the vapor film. It shows the bubbly flow and film flow upstream and downstream of the quench front, respectively. The quench front appears to reach the central and top regions of the test section at 38 s and 43 s, respectively. The high-speed camera pictures show details of the flow structure in the local region (approximately 40 mm in height) during a short period of time, i.e., 3 s. A thick and wavy film is formed on the hot surface of the cladding specimen before the quench front passes by. The bubbly flow follows the film flow upstream of the quench front as it moves upwards.

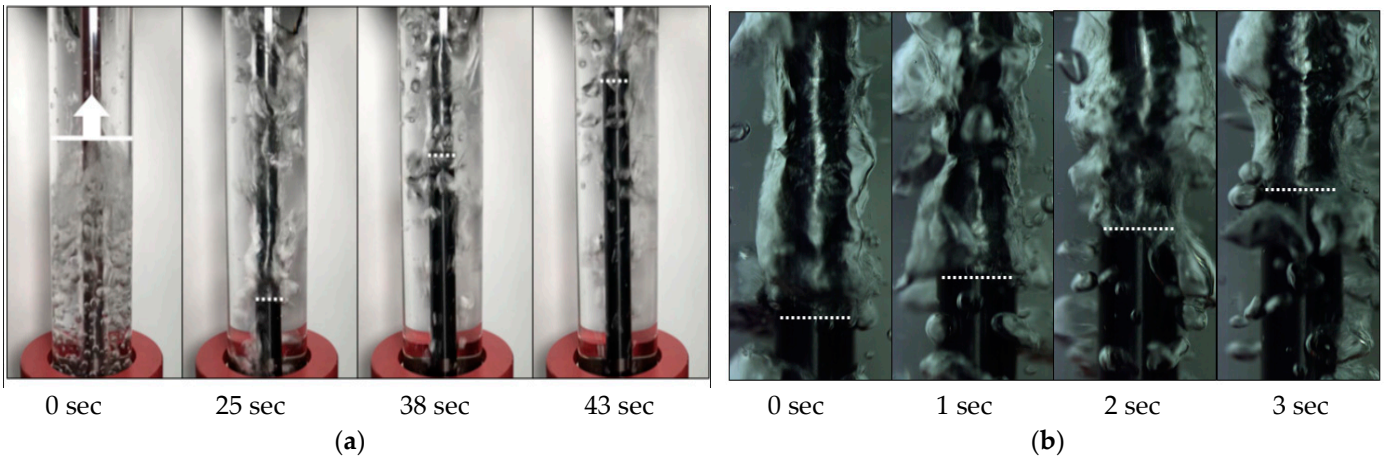

Figure 6. Pictures of the Zr cladding quenching at Tw = 800 °C, T_{sub} = 5 °C and Vc = 0.05 m/s using; (**a**) digital camera; (**b**) high-speed camera.

Figure 7 displays the flow visualization pictures for the CrAl-coated Zr quenching under the same test conditions as used for the Zr cladding, i.e., Tw = 800 °C, T_{sub} = 5 °C, Vc = 0.05 m/s. It shows a mixture of vapor film near the cladding surface and bubbly flow moving away from the surface. The quench front moves up from the bottom region at 11 s to the top region at 23 s. The high-speed pictures also show the film flow downstream of the quench front and bubbly/slug flow upstream. It should be noted that the vapor film appears to be a thinner and more turbulent wave than in the Zr cladding case.

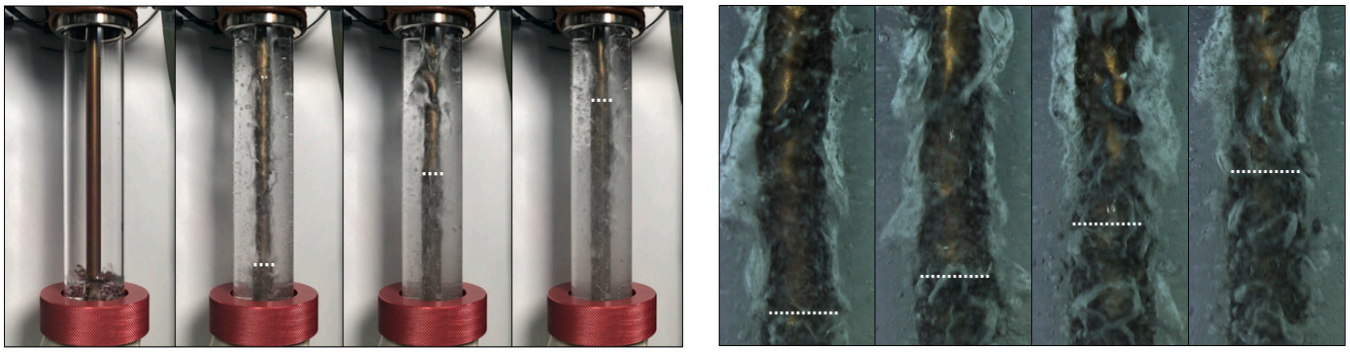

Figure 7. Pictures of the CrAl-coated Zr cladding quenching at Tw = 800 °C, T_{sub} = 5 °C and Vc = 0.05 m/s using; (**a**) digital camera; (**b**) high-speed camera.

Figures 8 and 9 show the quenching visualization of uncoated and CrAl-coated Zr claddings under high subcooling conditions, i.e., T_{sub} = 50 °C. The digital camera pictures show the water level in the test section marked by a white solid line. The pictures of the high-speed camera for 0.6 s show a stable and thin film on the cladding surface. The high-speed images also show clearly the quench front (dot line) moving upwards. The quench front for Zr cladding appears to be symmetric in circumferential direction as shown in Figure 8. The flow pattern and the speed of quench front appear to be almost same for uncoated and CrAl-coated Zr claddings. However, Figure 9 shows an asymmetric quench front for the CrAl-coated Zr cladding. This might be caused by non-uniform coating in Figure 4 and an unsmooth surface of CrAl-coated Zr cladding. Lee et al. [18] provided SEM images of CrAl-coated Zr cladding that show an unsmooth surface after polishing. It can be noted that the quench front at high subcooling is much faster than that at low subcooling. The top-down quenching was also observed under certain test conditions because of rapid cooling in the top portion of cladding specimen.

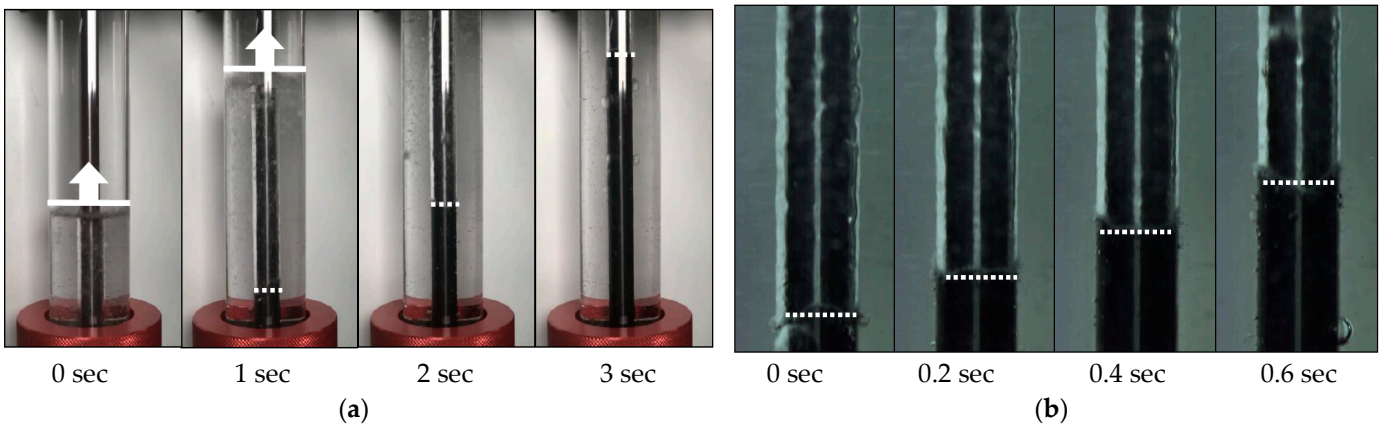

Figure 8. Pictures of the Zr cladding quenching at Tw = 800 °C, T_{sub} = 50 °C and Vc = 0.05 m/s using; (**a**) digital camera; (**b**) high-speed camera.

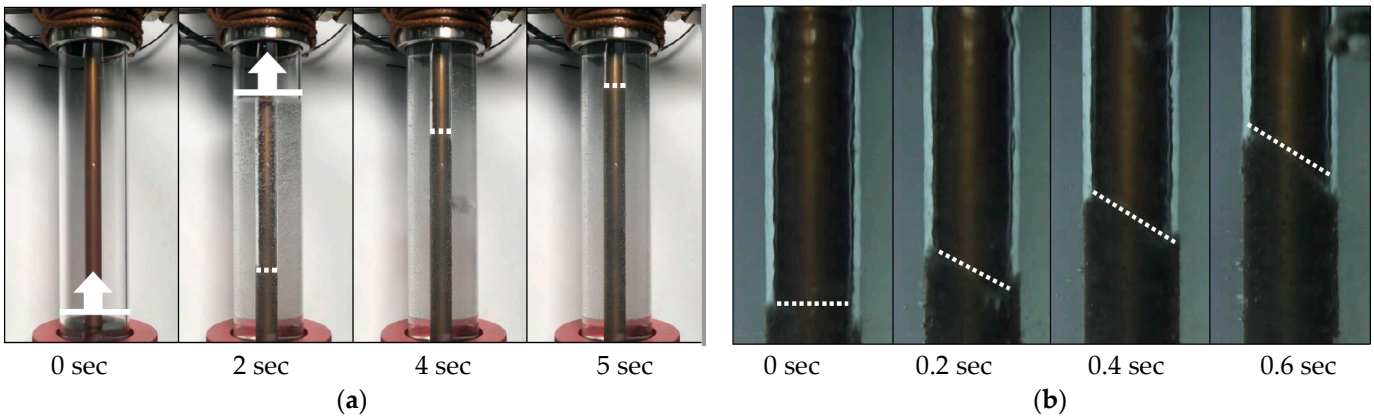

Figure 9. Pictures of the CrAl-coated Zr cladding quenching at Tw = 800 °C, T_{sub} = 50 °C and Vc = 0.05 m/s using; (**a**) digital camera; (**b**) high-speed camera.

3.2. Parametric Analysis of Quenching Curve

Figure 10 compares the quenching curves of three consecutive tests for Zr and CrAl-coated Zr claddings. The test conditions are 800 °C, 95 °C and 0.05 m/s for cladding temperature, coolant temperature and reflood velocity, respectively. The time scale for the quenching curve is adjusted such that it is 0.0 s when the coolant reaches the TC1 in bottom position. The error bar is plotted in the quench curves for the as-received specimens in order to show the measurement accuracy of cladding temperature (±3.7 °C). The quenching curves for the Zr specimen show a gradual decrease of cladding temperature (TC1) for 20 s after the coolant injection, i.e., in the film boiling regime. It shows a rapid decrease of cladding temperature after the transition to nucleate boiling. The quenching curves for the CrAl-coated Zr specimen also show the film boiling for approximately 15 s and the transition to nucleate boiling. The quenching curves for three test runs agree well with each other showing an excellent repeatability of this experiment.

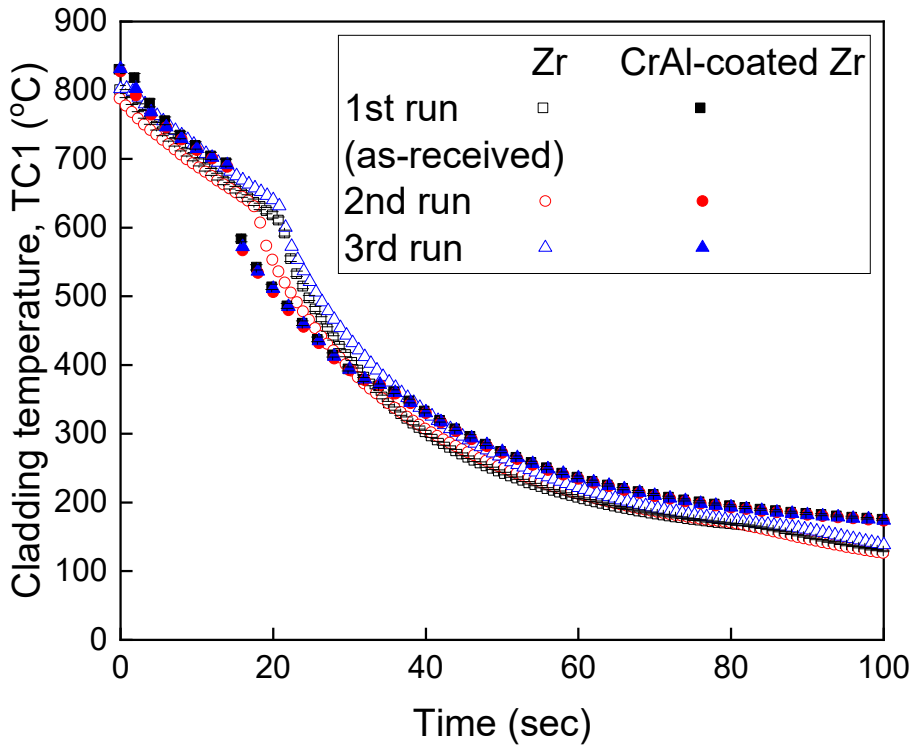

Figure 10. Repeatability of quenching tests for Zr cladding and CrAl-coated Zr cladding.

Figure 11 shows the quenching curve of the CrAl-coated Zr at Tw = 600 °C, T_{sub} = 5 °C and Vc = 0.05 m/s. It shows a gradual decrease of the cladding temperature due to film boiling in the early stages of quenching. The transition to nucleate boiling can be also seen in the quenching curve by the rapid drop in cladding temperature in between 10 s and 20 s. Figure 11b clearly shows the sequence of transition boiling from bottom to top of the cladding specimen. The cladding temperature at the bottom (TC1) and top (TC4) sections show the transition at 10 s and 16 s, respectively. It is also noted that the cladding temperature at the middle section (TC2 and TC3) indicates transition boiling at the same time, e.g., 14 s. The rewetting temperatures (RWTs) appear to be approximately 490 °C and 525 °C at the middle and bottom sections, respectively. The RWT is defined as the transition temperature from film boiling to nucleate boiling in this paper as indicated in Figure 11b.

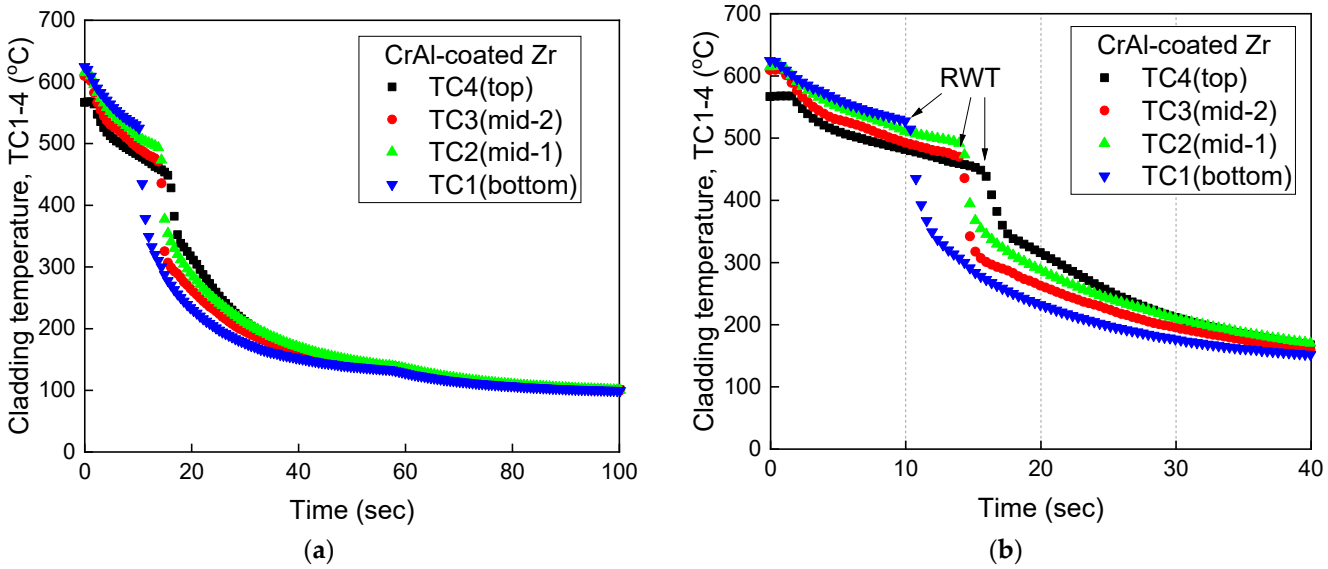

Figure 11. Quenching curve of the CrAl-coated Zr cladding at Tw = 600 °C, T_{sub} = 5 °C and Vc = 0.05 m/s; (**a**) overview; (**b**) zoom in view.

Figure 12 shows the effect of initial cladding temperature on the quenching curve for the CrAl-coated Zr cladding. The test specimen was heated to reach the initial target temperatures, i.e., 600 °C and 800 °C. It is noted that the cladding temperature in the top location (TC4) is slightly lower than at others (TC1 and TC2). The coolant subcooling was approximately 5 °C with the reflood velocity of 0.05 m/s. The quenching curves show a longer period of film boiling and higher RWTs as the cladding temperature increases. It is noted that the initial cladding temperature at the top section (TC4) is approximately 10% lower than those at the bottom and middle sections (TC1 & TC2). This is due to non-uniform heating of the cladding tube in the axial direction and higher heat loss to the top region. The RWT values in the middle (TC2) are approximately 494 °C and 655 °C for the cladding temperatures of 600 °C and 800 °C, respectively. The cooling rate of CrAl-coated Zr cladding in film boiling is estimated at 9.7 °C/s and 7.6 °C/s for Tw = 600 °C and Tw = 800 °C, respectively. Hence, the RWT increases but the cooling rate in film boiling regime decreases as the cladding temperature increases.

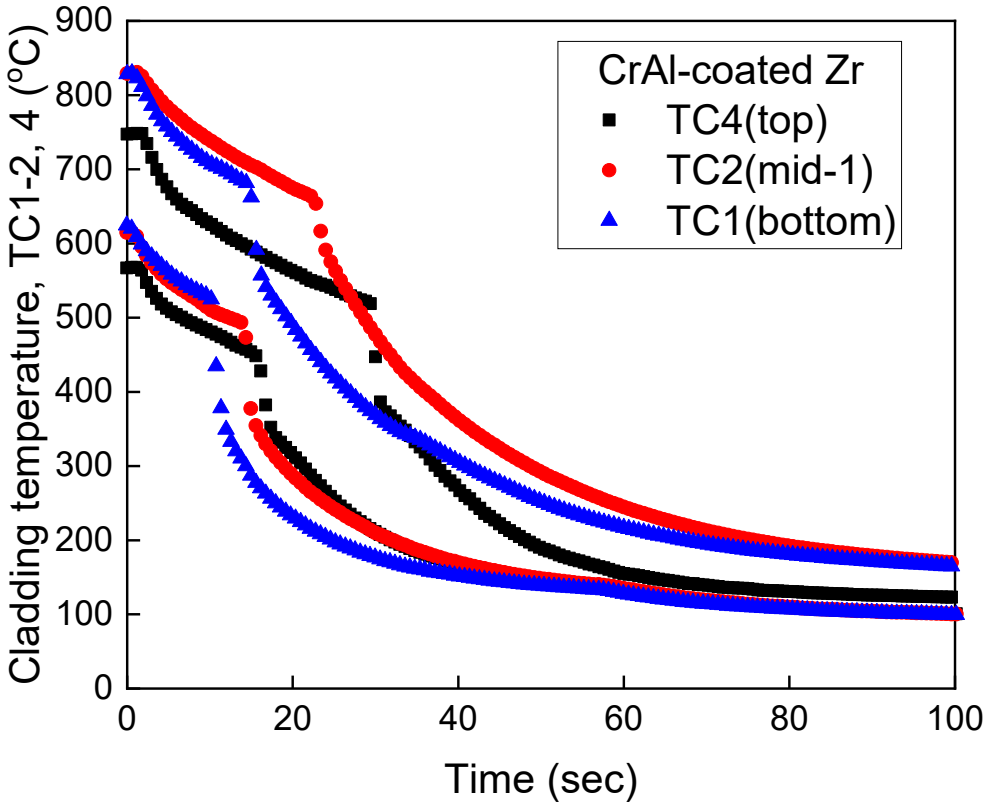

Figure 12. Effect of initial cladding temperature for the CrAl-coated Zr quenching at T_{sub} = 5 °C and Vc = 0.05 m/s.

Figure 13 shows the effect of reflood velocity on the quenching performance of CrAl-coated Zr cladding. The reflood velocity (Vc) was changed to 0.02, 0.05 and 0.1 m/s. The initial cladding temperature is 800 °C and the coolant subcooling is 7–15 °C for low subcooling and 50 °C for high subcooling. The low reflood velocity (Vc = 0.02 m/s) appears to result in faster cooling under low subcooling conditions in Figure 13a. This is because the coolant subcooling for low reflooding is higher than those for high reflooding cases. It should be noted that the coolant temperature is slightly different from the target value under the low subcooling conditions. Figure 13b compares the quenching curves at high subcooling, i.e., T_{sub} = 50 °C. It shows almost same quenching curves for the three reflooding cases. Therefore, the reflood velocity seems to have a minimal effect on quenching characteristics such as RWT and cooling rate in film boiling.

Figure 14 shows the effect of coolant subcooling for CrAl-coated Zr cladding. The initial cladding temperature is 600 °C and 800 °C with the constant reflood velocity of 0.05 m/s. The coolant subcooling ranges from 5 °C to 50 °C. The duration of film boiling decreases significantly as the coolant subcooling increases. The vapor film is very thin and disappears shortly after the coolant reflooding under high subcooling conditions, e.g., T_{sub} > 30 °C. The duration of film boiling is 10 s for the subcooling of 10 °C at Tw = 600 °C as shown in in Figure 14a. Figure 14b indicates the duration of film boiling for 14 s and 7 s for the subcooling at 10 °C and 20 °C, respectively. The RWT appears to increase significantly when the coolant subcooling is higher than 20 °C. Hence, the fast cooling is possible for the CrAl-coated Zr cladding if the coolant subcooling is higher than 20 °C.

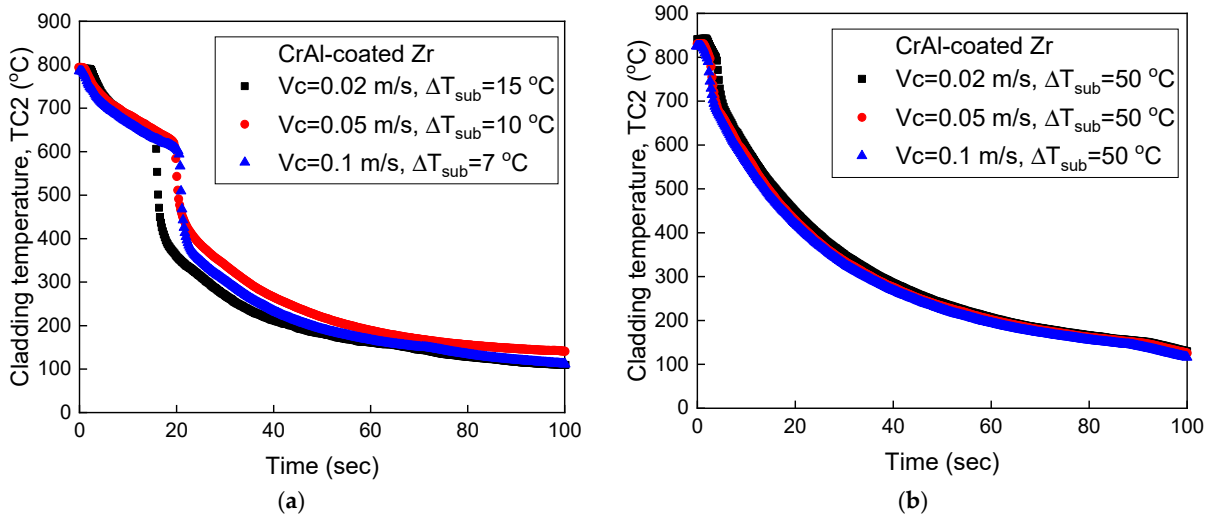

Figure 13. Effect of reflood velocity for the CrAl-coated Zr quenching at Tw = 800 °C; (**a**) low subcooling; (**b**) high subcooling.

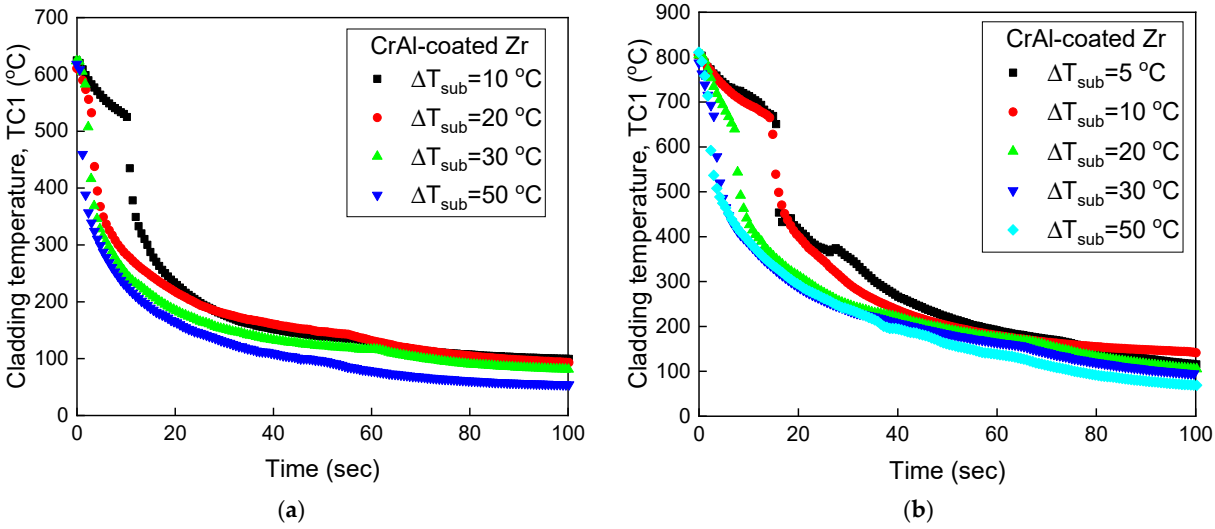

Figure 14. Effect of coolant subcooling for the CrAl-coated Zr quenching at; (**a**) Tw = 600 °C; (**b**) Tw = 800 °C.

Figure 15 compares the quenching curves of uncoated and CrAl-coated Zr specimens for initial cladding temperatures of 600 °C and 800 °C. In the case of high subcooling, e.g., T_{sub} = 50 °C, the cladding temperature decreases rapidly as soon as the coolant reflooding begins. This is because the thin film quickly collapses due to the quench front as shown in Figures 8 and 9. The CrAl-coated Zr cladding shows a cooling performance similar to the Zr cladding for high subcooling conditions. For the coolant subcooling of 10 °C and initial temperature of 600 °C seen in Figure 15a, the CrAl-coated cladding shows slightly slower cooling in film boiling regime than the Zr cladding. This seems to be the effect of the higher initial temperature of CrAl-coated Zr cladding. It is noted that the initial cladding temperature depends largely on the experimental conditions such as ambient temperature and heat loss. However, the CrAl-coated Zr cladding shows much faster cooling at T_{sub} = 5 °C and Tw = 800 °C in Figure 15b. The transition to nucleate boiling occurs at 20 s and 40 s for the CrAl-coated Zr and the Zr, respectively. The faster cooling at high temperature and low subcooling for CrAl-coated Zr cladding attributes to smaller contact angle and higher surface roughness.

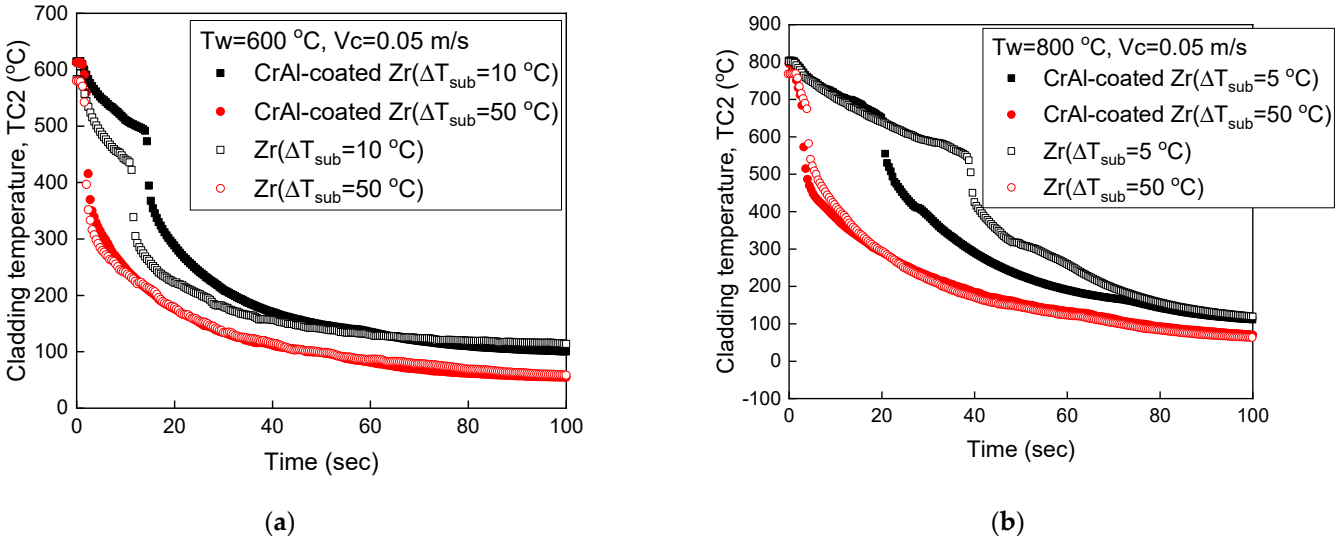

Figure 15. Comparison of quenching curves for Zr and CrAl-coated Zr at; (**a**) Tw = 600 °C; (**b**) Tw = 800 °C.

3.3. Quenching Performance of CrAl-Coated Zr Cladding

Figure 16 compares the measurements of rewetting temperature with the previous correlations. The RWT measured in this experiment is obtained from the quenching curve of the cladding temperature at the bottom (TC1). The measurement error for RWT is estimated at ±25 °C and ±40 °C for the Zr and the CrAl-coated Zr, respectively. This error is estimated from the variation of cladding temperature during the time interval of data acquisition (±0.2 s) during transition boiling. The RWT increases as the coolant subcooling and/or initial cladding temperature increases. There is no significant difference in RWT between the Zr cladding and the CrAl-coated Zr cladding.

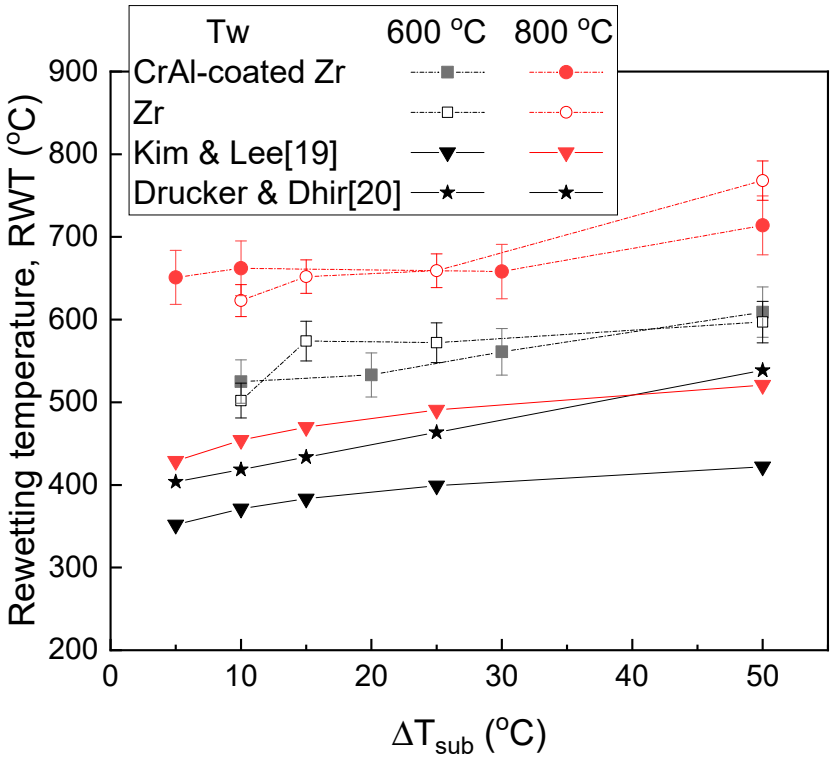

Figure 16. Comparison of rewetting temperature for Zr and CrAl-coated Zr claddings.

The RWT correlations used in this study are those of Kim and Lee [19], and Drucker and Dhir [20]. Kim and Lee [19] proposed the prediction correlation of apparent rewetting temperature (T_{AR}) in Equation (1) under the bottom flooding conditions of vertical circular tubes:

$$T_{AR} = 19.51(T_w - T_{sat})\left(\frac{T_{sat} - T_f}{T_w - T_{sat}}\right)^{0.107}\left(\frac{c_{p.w}G\delta}{k_w}\right)^{-0.162}\left[\frac{k_w\rho_w^2(T_w - T_{sat})}{\delta G^3}\right]^{-0.0989}\left(\frac{z}{\delta}\right)^{-0.163} \quad (1)$$

where, T_w, T_{sat}, and T_f are the wall temperature, saturation temperature, and coolant temperature, respectively. $c_{p.w}$, k_w, and ρ_w are the specific heat, thermal conductivity, and density of test tube, respectively. δ, G, and z are the tube wall thickness, liquid mass flux, and axial distance from the inlet, respectively.

Drucker and Dhir [20] conducted quenching experiments using a rod bundle with four Zircaloy test specimens. They developed the correlation of quenching temperature (T_Q) considering the effects of flooding velocity and coolant subcooling given in Equation (2):

$$T_Q = 550 + 50\sqrt{U} + 3\Delta T_{sub} \quad (2)$$

where, U indicates the flooding velocity and ΔT_{sub} is the coolant subcooling.

The RWT correlations in Figure 16 show the increase of RWT (T_{AR} or T_Q) as the coolant subcooling increases. The Kim and Lee correlation also shows the increase of RWT as the initial specimen temperature increases. The measured RWTs in this experiment are somewhat higher than the correlation predictions. This is because the TCs appear to be in incomplete contact with the cladding tube caused by thermal expansion and shrinkage during quenching test. However, the dependence of RWT on initial specimen temperature and coolant subcooling is consistent with the correlations.

Figure 17 compares the speed of quench front depending on coolant subcooling for uncoated and CrAl-coated Zr claddings. The initial cladding temperatures are 600 °C and 800 °C with the reflood velocity of 0.05 m/s. The speed of quench front (V_{QF}) is estimated by accounting for traveling time from the bottom TC (TC1) to the top TC (TC4) as follows:

$$V_{QF} = \frac{\Delta z}{\Delta t} \quad (3)$$

where, Δz is the distance between TC1 and TC4, i.e., 0.08 m. Δt is the difference in rewetting time between TC1 and TC4. The measurement error in the quench front velocity is 4% and 20% at low subcooling and high subcooling, respectively. The speed of the quench front can also be estimated by analyzing the progress of the quench front in high-speed camera images.

The speed of the quench front increases significantly as the coolant subcooling increases. However, it decreases as the initial specimen temperature increases. Stepanek et al. [21] also found the same dependence of quench front velocity on coolant subcooling and initial temperature from the reflood quenching of stainless steel (SS) rod. The quench front velocity of this experiment agrees well with the previous experimental data of Seshadri and Shirvan [13], and Stepanek et al. [21], as shown in Figure 17. The CrAl-coated Zr appears to show slightly higher quench front velocity than the Zr at Tw = 800 °C. However, the quench front velocity of CrAl-coated Zr is lower than the Zr one at Tw = 600 °C. Hence, it can be judged that the quench front velocity of CrAl-coated Zr is comparable to the Zr result.

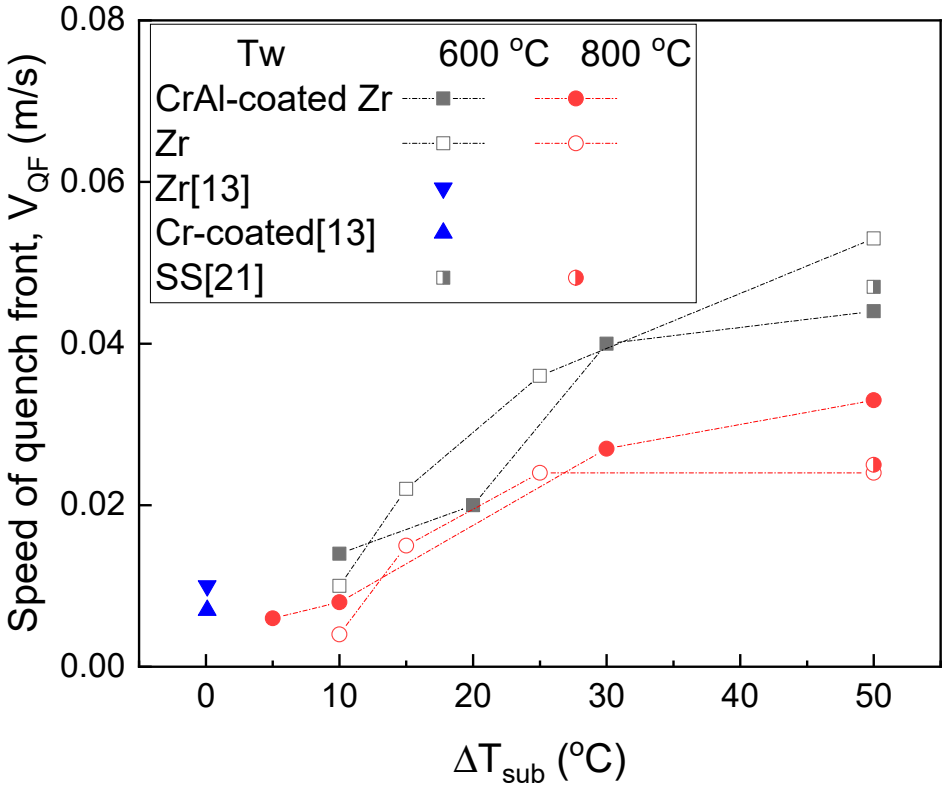

Figure 17. Speed of quench front for Zr and CrAl-coated Zr claddings.

4. Conclusions

A reflood quenching experiment was conducted to evaluate the cooling performance of accident-tolerant cladding, i.e., CrAl-coated Zr tube against the commercial Zr tube. The experimental conditions are an initial tube temperature of 600 °C and 800 °C, the coolant subcooling from 5 °C to 50 °C and the reflood velocity from 0.02 m/s to 0.1 m/s. The flow pattern and quenching curve are compared for CrAl-coated Zr and Zr tube specimens. The contact angle, rewetting temperature and quench front velocity are also compared to evaluate the quenching performance of CrAl-coated Zr cladding. The findings of this quenching experiment can be summarized as below:

(1) The CrAl-coated Zr cladding shows the flow pattern and heat transfer mode similar to the uncoated Zr cladding during reflood quenching. The vapor film for the CrAl-coated Zr specimen shows thinner and more turbulent wave than the Zr one at low subcooling. At high subcooling, the CrAl-coated Zr cladding shows asymmetric quench front that moves upwards quickly.

(2) The quenching curves for the high subcooling condition do not show any noticeable difference between uncoated Zr and CrAl-coated Zr claddings. The CrAl-coated Zr specimen shows fast quenching with high RWT and high speed of quench front at high initial cladding temperature (Tw = 800 °C) and low subcooling ($T_{sub} \leq 10$ °C).

(3) The RWT increases as the coolant subcooling and/or initial cladding temperature increases. The reflood velocity has a negligible effect on RWT. There is no significant difference in RWT between the Zr cladding and the CrAl-coated Zr cladding.

(4) The quench front velocity of CrAl-coated Zr is slightly higher than the Zr one at low subcooling but becomes lower at high subcooling and low initial wall temperature. Hence, it can be concluded that the quench front velocity of CrAl-coated Zr is comparable to the Zr result.

(5) The CrAl-coated Zry-4 cladding is quite promising for the ATF candidate which can result in acceptable quenching performance as well as suppression of hydrogen

generation in the event of no active cooling in LWR. The future work is necessary to measure the film thickness and conduct the quenching experiment at initial wall temperature higher than the peak cladding temperature limit of LOCA.

Author Contributions: Conceptualization, W.K.I.; methodology, W.K.I.; validation, W.K.I.; formal analysis, W.K.I.; investigation, W.K.I.; resources, W.K.I.; data curation, K.G.L.; writing—original draft preparation, W.K.I.; writing—review and editing, W.K.I.; visualization, K.G.L.; supervision, W.K.I.; project administration, W.K.I.; funding acquisition, W.K.I. All authors have read and agreed to the published version of the manuscript.

Funding: This research was funded by National Research Foundation in Rep. of Korea, grant number 2017M2A8A5015058 and China-Korea cooperation project, grant number 72702-19.

Institutional Review Board Statement: Not applicable.

Informed Consent Statement: Not applicable.

Data Availability Statement: Not applicable.

Acknowledgments: This work was supported by a National Research Foundation of Korea (NRF) grant funded by the Korea government (MSIP) (No. 2017M2A8A5015058) and the China-Korea cooperation project. The authors thank to cladding development team in KAERI for providing test specimens.

Conflicts of Interest: The authors declare no conflict of interest. The funders had no role in the design of the study; in the collection, analyses, or interpretation of data; in the writing of the manuscript, or in the decision to publish the results.

References

1. Zinkle, S.J.; Terrani, K.A.; Gehin, J.C.; Ott, L.J.; Snead, L.L. Accident tolerant fuels for LWRs: A perspective. *J. Nucl. Mater.* **2014**, *448*, 374–379. [CrossRef]
2. Kurata, M. Research and development methodology for practical use of accident tolerant fuel in light water reactors. *Nucl. Eng. Technol.* **2016**, *48*, 26–32. [CrossRef]
3. Yueh, K.; Terrani, K.A. Silicon carbide composite for light water reactor fuel assembly applications. *J. Nucl. Mater.* **2014**, *448*, 380–388. [CrossRef]
4. Snead, L.L.; Terrani, K.A.; Katoh, A.; Silva, C.; Leonard, K.J.; Perez-Berquist, A.G. Stability of SiC-matrix microencapsulated fuel constituents at relevant LWR conditions. *J. Nucl. Mater.* **2014**, *448*, 389–398. [CrossRef]
5. Terrani, K.A.; Zinkle, S.J.; Snead, L.L. Advanced oxidation-resistant iron-based alloys for LWR fuel cladding. *J. Nucl. Mater.* **2014**, *448*, 420–435. [CrossRef]
6. Yan, Y.; Keiser, J.R.; Terrani, K.A.; Bell, G.L.; Snead, L.L. Post-quench ductility evaluation of Zircaloy-4 and select iron alloys under design basis and extended LOCA conditions. *J. Nucl. Mater.* **2014**, *448*, 436–440. [CrossRef]
7. Nelson, A.T.; Sooby, E.S.; Kim, Y.-J.; Cheng, B.; Maloy, S.A. High temperature oxidation of molybdenum in water vapor environments. *J. Nucl. Mater.* **2014**, *448*, 441–447. [CrossRef]
8. Koyanagi, T.; Ozawa, K.; Hinoki, T.; Shimoda, K.; Katoh, Y. Effects of neutron irradiation on mechanical properties of silicon carbide composites fabricated by nano-infiltration and transient eutectic-phase process. *J. Nucl. Mater.* **2014**, *448*, 478–486. [CrossRef]
9. Ott, L.J.; Robb, K.R.; Wang, D. Preliminary assessment of accident-tolerant fuels on LWR performance during normal operation and under DB and BDB accident conditions. *J. Nucl. Mater.* **2014**, *448*, 520–533. [CrossRef]
10. Ben-Belgacem, M.; Richet, V.; Terrani, K.A.; Katoh, Y.; Snead, L.L. Thermo-mechanical analysis of LWR SiC/SiC composite cladding. *J. Nucl. Mater.* **2014**, *447*, 125–142. [CrossRef]
11. Pint, B.A.; Terrani, K.A.; Brady, M.P.; Cheng, T.; Keiser, J.R. High temperature oxidation of fuel cladding candidate materials in steam–hydrogen environments. *J. Nucl. Mater.* **2013**, *440*, 420–427. [CrossRef]
12. Kim, H.G.; Kim, I.H.; Jung, Y.I.; Park, D.J.; Park, J.H.; Choi, B.K.; Lee, Y.H. Out-of-pile performance of surface-modified Zr cladding for accident tolerant fuel in LWRs. *J. Nucl. Mater.* **2018**, *510*, 93–99. [CrossRef]
13. Seshadri, A.; Shirvan, K. Quenching heat transfer analysis of accident tolerant coated fuel cladding. *Nucl. Eng. Des.* **2018**, *338*, 5–15. [CrossRef]
14. Lee, S.K.; Liu, M.; Brown, N.R.; Terrani, K.A.; Blandford, E.D.; Ban, H.; Jensen, C.B.; Lee, Y. Comparison of steady and transient flow boiling critical heat flux for FeCrAl accident tolerant fuel cladding alloy, Zircaloy, and Inconel. *Int. J. Heat Mass Transf.* **2019**, *132*, 643–654. [CrossRef]
15. Kang, J.Y.; Kim, T.K.; Lee, G.C.; Kim, M.H.; Park, H.Y. Quenching of candidate materials for accident tolerant fuel-cladding in LWRs. *Ann. Nucl. Energy* **2018**, *112*, 794–807. [CrossRef]

16. Wang, Z.; Xiong, J.; Yao, W.; Qu, W.; Yang, Y. Experimental investigation on the Leidenfrost phenomenon of droplet impact on heated silicon carbide surfaces. *Int. J. Heat and Mass Transf.* **2019**, *128*, 1206–1217. [CrossRef]
17. Wang, Z.; Zhong, M.; Deng, J.; Liu, Y.; Huang, H.; Zhang, Y.; Xiong, J. Experimental investigation on the transient film boiling heat transfer during quenching of FeCrAl. *Ann. Nucl. Energy* **2021**, *150*, 107842. [CrossRef]
18. Lee, K.G.; In, W.K.; Kim, H.G. Quenching experiment on Cr-alloy-coated cladding for accident-tolerant fuel in water pool under low and high subcooling conditions. *Nucl. Eng. Des.* **2019**, *347*, 10–19. [CrossRef]
19. Kim, A.K.; Lee, Y. A correlation of rewetting temperature. *Lett. Heat Mass Transf.* **1979**, *6*, 117–123. [CrossRef]
20. Drucker, M.; Dhir, V.K. *Effects of High Temperature and Flow Blockage on the Reflood Behavior of a 4-Rod Bundle*; EPRI Report, NP-2122; EPRI: Washington, DC, USA, 1981.
21. Stepanek, J.; Blaha, V.; Dostal, V. Quench front propagation in the annular channel. *Acta Polytech. CTU Proc.* **2016**, *4*, 97–101. [CrossRef]